

UNIVERSIDAD DE SANTIAGO DE COMPOSTELA



FACULTAD DE FÍSICA
Departamento de Física de Partículas

Accurate calculation of the optical transmission of high resolving spectrometer

Memoria presentada por:

Dušan Dragosavac

como

Trabajo de Investigación Tutelado

dentro del **Programa de Doctorado**

Interuniversitario en Física Nuclear

Julio 2009

UNIVERSIDAD DE SANTIAGO DE COMPOSTELA

Jose Benlliure Anaya, Profesor Titular de la Universidad de Santiago de Compostela

CERTIFICA: que la memoria titulada **Accurate calculation of the optical trans-mission of high resolving spectrometer** ha sido realizada por **Dušan Dragosavac** en el **Departamento de Física de Partículas de esta Universidad** bajo mi dirección y constituye el **Trabajo de Investigación Tutelado** dentro del **Programa Interuniversitario de Física Nuclear** que presenta para optar al **Diploma de Estudios Avanzados**.

Santiago de Compostela, 22 de Julio de 2009

Fdo: Jose Benlliure Anaya

Fdo: Dušan Dragosavac

Contents:

Introduction	1
1 Physics of Ion optics	3
1.1 Charged particle beams	3
1.2 Phase space	4
1.3 Liouville's theorem	5
1.4 Spectrometers	7
1.4.1 Dipoles	7
1.4.2 Quadrupoles	9
1.4.3 Sextupoles	10
2 Transmission through the Fragment Separator	11
2.1 The Fragment Separator	11
2.2 Beam without dispersions	13
2.3 Beam with transversal momentum dispersions: fragmentation reactions	13
2.4 Beam with transversal momentum dispersions: fission reactions	14
3 MOCADI – Monte Carlo code for the transport of heavy ions through matter within ion-optical systems	16
3.1 Interaction of heavy ions with matter	16
3.2 Nuclear interactions	16
3.3 Atomic interactions	17
3.4 Transport through matter within ion-optical systems	18
3.5 Structure and application of the code MOCADI	18

4 Simulation and analysis	19
4.1 MOCADI simulation for calculating transmission of FRS from S2 to S4	19
4.2 Correlation between position and angular distributions	22
4.2.1 Position distribution at S2	22
4.2.2 Angular distributions in x	23
4.2.3 Angular distributions in y	23
4.2.4 Transmission and restrictions in distribution's width	25
4.3 Evaluation of simulation results	27
4.3.1 Transmission and deviation from the mean position of distribution at S2	27
4.3.2 Transmission and width of distribution at S2	28
4.3.3 Transmission and mean position of distribution at S4	29
5 Summary and conclusions	32
6 Appendix	35
Bibliography	38

Introduction

Magnetic spectrometers are largely used in experimental nuclear physics. These devices allow one to perform precise measurements of the reaction kinematics or to separate and fully identify the reaction residues for nuclear-dynamics and structure studies. They can also be used as separators to produce radioactive nuclear beams. There are many such devices at modern experimental facilities throughout the world, e.g. GSI [1], RIKEN [2], GANIL [3] and others. Reactions using radioactive beams provide various features that are not available with beams of stable nuclei. Experiments with radioactive beams allow studying the nuclear properties of exotic nuclei like total interaction cross sections, production cross sections, momentum distribution calculations and many others with high accuracy. However, all these applications are effected by the limited transmission of the reaction residues through the spectrometer.

The final transmission depends on the ion optical characteristics and the mechanical constraints of the spectrometer but also on the kinematical properties of the considered nuclei. The ion optics is characterized by the bending (dispersion) and focusing (magnification) powers of the magnetic elements which constitute the spectrometer. The reaction mechanism determines the kinematics of the particles.

The transmission losses in any magnetic spectrometer can be attributed to its limited acceptance in longitudinal momentum and angle. The limitation in longitudinal momentum can be overcome by combining different magnetic settings. In the case of a zero-degree spectrometer, the angular acceptance can only be estimated with calculations.

Standard ion-optical transport codes (TRANSPORT [4], MOCADI [5], GICO [6]) are commonly used to determine the transmission of charged particles through magnetic spectrometers. By using Monte-Carlo code MOCADI we have performed a comprehensive study of the transmission at FRagment Separator (FRS) [7]. The aim was to get a systematic view on transmission of the second part of FRS in order to accurate calculations. In this work we present a method to parameterize measured and simulated distributions at focal planes of FRS using moments of 1st to 4th order. The idea is to find a way to enable quantitative

comparison of these distributions and to evaluate the transmission with the deviation in these moments between measured and simulated distributions.

This work is organized as follows. In chapter 1 we describe the physics of ion-optics introducing optical phase space and transport of charged particle through the magnetic spectrometer. Chapter 2 is devoted to the FRS and dispersion in the momentum and angular distribution for fragmentation and fission reactions. In section 3 we describe the MOCADI code which we are going to use for calculating the transmission. In the final chapter the results of our simulations and conclusions are presented.

Chapter 1

Physics of Ion optics

1.1 Charged particle beams

Experiments in nuclear and high energy physics use beams of charged particles as probes to explore the structure of nuclei. Magnetic fields are used to guide the beam to and focus it onto the target where the reaction being studied takes place. The reaction products are collected and may be analyzed by additional magnetic fields.

The optics of charged particle beams is the science of using magnetic fields to bend and direct the paths of a group of moving charged particles [8]. A beam of particles can be influenced in a manner analogous to the focusing of light by an optical lens or the dispersion into colors by a prism. It may be changed in direction, brought together to a small spot or have its particle selected by momentum. The beam line components are different types of magnets with their fields oriented perpendicularly to the direction of motion of the particle beam.

Roughly speaking, a collection of moving charged particles constitutes a beam when the particles are all moving in the same direction with nearly the same momentum and have a small separation transverse to the general direction of motion. We refer to momentum instead of velocity or kinetic energy since it is momentum which appears in the equations of motion. The range of momenta may vary from tens of percent in a nuclear physics analyzing spectrometer to tenths of a percent in a beam extracted from an accelerator. The angular divergence may be a few degrees in each transverse direction at tens of MeV, or only a fraction of a miliradian in a particle beam at hundreds of GeV. Finally, the spatial extent of the ensemble must be small enough to pass through the apertures of the magnets, which is the region of space where the magnetic field occurs which is used to deflect and focus the beam.

A charged particle in a magnetic field B experienced a force F which is given by the expression

$$\vec{F} = q\vec{v} \times \vec{B} \quad (1.1)$$

Here q is the charge of the particle and v is the velocity. The direction of the force is perpendicular to both the velocity vector and the magnetic field. It is greatest when the velocity vector is perpendicular to the magnetic field. Since force is the derivative of momentum and velocity is the time derivative of position

we can use equation (1.1) to formulate a differential equation to find the particle's position as a function of time.

In charged particle optics, however, we are not so much interested in finding a particle's position as a function of time as in determining the path it follows. The independent variable is then taken to be distance along a particular one of many trajectories passing down the beam line.

In a uniform magnetic field, a charged particle whose velocity vector is perpendicular to the field moves in a circular path. The radius ρ of the circle is related to the momentum p of the particle, the charge q and the strength of the field B by

$$\vec{p} = q\vec{B}\rho \quad (1.2)$$

1.2 Phase space

A beam of particles at any instant of time may be represented by a collection of points in a six dimensional space, known as phase space [9]. The phase space location of a single particle has three coordinates specifying the position of the particle and three giving its momentum. The last three coordinates alone make up what we shall refer to as momentum space.

$$\vec{P} = (x, p_x, y, p_y, z, p_z)$$

This point defines all the properties of the particle. In principle, if we know the forces acting inside an ion-optical device, we can exactly reconstruct the classical equation of motion of the particle through the elements of the optical system.

In this sense, an optical system can be regarded as a box in which the relation between the properties at the entrance and the properties at the exit is defined. The system transforms the input values of the particle into some output values and vice-versa. The function which defines the transformation is biunique. So, all what is happening in between the entrance and the exit can be put in a system of equations. The solution of this system of equations gives a function f :

$$\begin{pmatrix} x^{exit} \\ p_x^{exit} \\ y^{exit} \\ p_y^{exit} \\ z^{exit} \\ p_z^{exit} \end{pmatrix} = f \cdot \begin{pmatrix} x^{entrance} \\ p_x^{entrance} \\ y^{entrance} \\ p_y^{entrance} \\ z^{entrance} \\ p_z^{entrance} \end{pmatrix} \quad (1.3)$$

The solution of the system of equations can be very complicated. One can develop it in series of powers and decide to which order of precision to extend the

calculation. If one stops at the first order, one does not have mixed terms that means the function f can be expressed as a 6×6 matrix of coefficients a_{ij} :

$$f = \begin{pmatrix} a_{11} & a_{12} & a_{13} & a_{14} & a_{15} & a_{16} \\ a_{21} & a_{22} & a_{23} & a_{24} & a_{25} & a_{26} \\ a_{31} & a_{32} & a_{33} & a_{34} & a_{35} & a_{36} \\ a_{41} & a_{42} & a_{43} & a_{44} & a_{45} & a_{46} \\ a_{51} & a_{52} & a_{53} & a_{54} & a_{55} & a_{56} \\ a_{61} & a_{62} & a_{63} & a_{64} & a_{65} & a_{66} \end{pmatrix} \quad (1.4)$$

that gives, for example,

$$x^{exit} = a_{11} \cdot x^{entrance} + a_{12} \cdot p_x^{entrance} + a_{13} \cdot y^{entrance} + a_{14} \cdot p_y^{entrance} + a_{15} \cdot z^{entrance} + a_{16} \cdot p_z^{entrance}$$

In the first-order calculation, a_{ij} are just coefficients; in higher-order calculations a_{ij} are functions of (x, p_x, y, p_y, z, p_z) .

1.3 Liouville's theorem

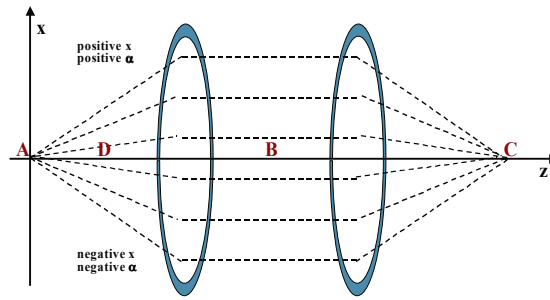
According to Liouville's theorem, if the forces acting inside the ion-optical system are conservative, then the volume in phase space occupied by the particles is conserved. This volume is called **emittance**. The analysis of the system can be anyhow divided in steps: in those sections where all the elements are conservative the emittance does not change, in those pieces where there are non-conservative forces one has to calculate how the emittance is changed. This new emittance goes as input for the next section.

A real ion-optical apparatus in general does not transmit all (for example, it cuts in angle or in momentum) and the volume in phase space which can pass is called **acceptance**. If the emittance is smaller than the acceptance then the transmission is 100%.

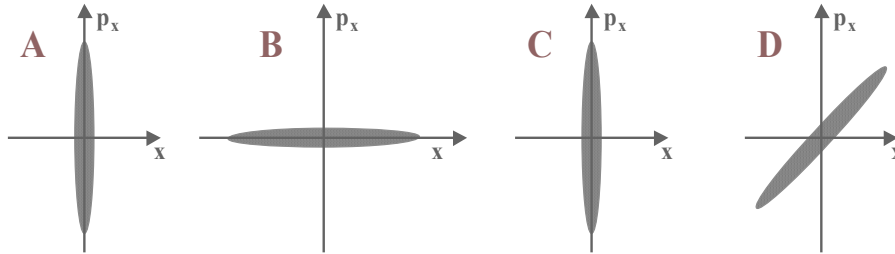
To see how the shape of the emittance can change, we make an example. Let's consider a very simple two-dimensional system in normal optic: a monochromatic light source and two lenses. The source is placed at the focus of the first lens (**A**), so the rays coming out of the lens will be parallel (**B**). The image is formed in point (**C**). Similarly we can consider a mono-energetic beam going in the z direction. In the ion-optic community the angle of the particle is defined as:

$$\alpha = x' = \frac{p_x}{p_z} \propto p_x \quad (1.5)$$

α is proportional to p_x , since p_z is constant.

Figure 1.1 – Emittance at x points A, B, C, D

We can represent the emittance in x at points A, B, C, D

Figure 1.2 – Emittance in x at points A, B, C, D

In point A, we have a very small beam-spot, but we have a spread in the momentum, because of the spread in the angle. In point B the situation is exactly the opposite, only few angles (all the rays are parallel) but many positions. In point D we have both many positions and many angles. The emittance (volume of the ellipse representing the occupied volume in the phase space) is anyhow always constant.

The example we have shown is meaningful because it respects the Liouville's theorem. On the other hand, in ion-optics, one often says that "if you accelerate a beam the emittance shrinks, and if you decelerate it, the emittance blows up". This seems to be a contradiction to the Liouville's theorem, but the reason is that in ion-optic conventions the phase space is defined in a different way, because one prefers to use the angles instead of the momenta.

The real (physically meaningful) phase space is defined by the following coordinates:

$$\Omega_{real} = (x, p_x, y, p_y, z, p_z) \quad (1.6)$$

but the ion-optic (physically not-meaningful) phase space is defined by the following coordinates:

$$\Omega_{ion-optic} = \left(x, \frac{p_x}{p_z}, y, \frac{p_y}{p_z}, z, \frac{\Delta p_z}{p_z} \right) = (x, x', y, y', z, \delta p_z) \quad (1.7)$$

where $\delta p_z = \Delta p_z/p_z$ represents the relative variation of magnetic rigidity when there is only one charge species.

Now, if we accelerate a beam, the momentum p_z increases, and the angles decrease, so the emittance shrinks (vice-versa if we decelerate it).

1.4 Spectrometers

A spectrometer is used to determine the direction, kinetic energy and particle type of the reaction products. The design of spectrometers varies according to the number of simultaneous reaction products it is to transmit and detect. At energies in the tens of GeV and above, reactions may yield a multiplicity of particles. A multiparticle spectrometer often consists of a single magnet with a large opening with respect to the length, where detectors are placed both before and after the magnet to register the passage of particles (ALADIN [10]). The magnet can accept at once many particles with a large range of magnetic rigidities and different incoming angles; they will follow different paths and exit on different positions. So, no "standard" or "optimum" bending angle is defined. By detecting at least three points (two before and one after or vice-versa) of their trajectory, their magnetic rigidity can be deduced. Single particle spectrometers and beam lines usually contain several magnets (FRS [7]); a dipole is a curved long tunnel with an opening much smaller than its length. Therefore, only particles with a limited range of bending radii, centered around ρ_0 , can pass. The acceptance in angle is rather limited, too. The bending radius ρ_0 is defined by the geometry of the magnet. The magnets bend the trajectories of the particles and focus the beam. The spectrometer is designed to transmit and detect single particles from reactions in the target. Particle directions, momenta, charge and mass can be determined by the use of detectors placed both before, after and between the magnets.

Many different shapes and sizes of magnets are used in beam lines and spectrometers. In the following sections will be explained more about dipoles and quadrupoles.

1.4.1 Dipoles

A magnetic dipole is the ion optical equivalent of a prism. The field of the dipole is uniform across the aperture in the central region in the central region of the magnet, since the pole faces are flat and parallel. A dipole or bending deflects all trajectories of particles with a given charge in the same direction.

The equations that rule the motion of a particle (with charge q and mass m) are given combining the 2nd law of dynamics and the Lorentz force:

$$\frac{d}{dt}(m \cdot \vec{v}) = m_0 \cdot \frac{d}{dt}(\gamma \cdot \vec{v}) = q \cdot \vec{v} \times \vec{B} \quad (1.8)$$

Note that $m = \gamma \cdot m_0$ with $\gamma = \sqrt{(1 - \beta^2)^{-1}}$ and $\beta = |v|/c$ is velocity dependent. Since the force in a magnetic field is perpendicular to the velocity, then the net effect is a change in the particle direction, but the particle is not accelerated or decelerated.

If \vec{B} and \vec{v} are uniform and perpendicular to each other than it comes:

$$B\rho = \frac{m_0 \cdot \gamma \cdot v}{q} = \frac{p}{q} \quad (1.9)$$

where ρ is the bending radius of the trajectory. The ratio p/q ($= B\rho$) is called **magnetic rigidity** and it is a characteristic of a particle with a certain mass, charge and velocity.

The purpose of dipoles is as follows:

a) to identify a charged particle's

Once $B\rho$ is known by measuring the trajectory of the ion, the identification of the A/Z of a charged particle is easily done if an independent measurement of the velocity can be done. We exploit this equation:

$$\frac{A}{Z} = \frac{B\rho}{c \cdot \beta \cdot \gamma} \quad (1.10)$$

with $c\beta\gamma$ known from another source.

b) to evaluate the velocity of a fixed charged particle (selection of momentum)

Once $B\rho$ is known by the measurement of the trajectory of the ion, the evaluation of the velocity can be done if the A/Z of the charged particle is already known. We exploit the usual equation:

$$c \cdot \beta \cdot \gamma = \frac{B\rho}{A/Z} \quad (1.11)$$

The **dispersion** is a quantity that connects the variation of the position of an ion, bent by a magnet, with the variation of its magnetic rigidity. So two identical ions (i.e. same Z and A) that enter the magnet with different momenta (velocities) will follow different paths and land in different positions of a given plane. The dispersion can be defined as the transversal distance between a reference trajectory

and the trajectory of a particle with $\delta(B\rho) = \Delta(B\rho)/(B\rho) = 1\%$. It is expressed in cm/%.

Actually in the most general case (real magnet) the position where an ion lands depends on many factors (e.g. the angle, the path through the magnetic field). For this reason it is more correct to define the dispersion as the partial derivative with respect to the variation of the momentum of the ion:

$$D(\theta, \rho, B, \dots) = \frac{\partial x}{\partial p/p} \quad (1.12)$$

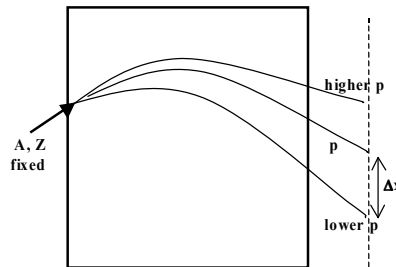


Figure 1.4 – Momentum dispersion of the ion

1.4.2 Quadrupoles

A pair of quadrupoles with a drift section in between is the ion-optical equivalent of a lens. In an experiment it is very practical to have a device in which the particles with the same magnetic rigidity but different incoming angle land in the same position (so that a measure of the position is directly a measure of the magnetic rigidity). This is done with the help of a quadrupoles which have properties **to focus** particles, i.e. to collect particles that are equal in rigidity but not in angle.

A focalizing lens is realized with two quadrupoles, rotated of 90° and separated by some distance (drift section). A quadrupole is a magnetic element with 4 poles, shaped in such a way that the intensity of the magnetic field increases linearly from center to the pole. So: $|B_x| \sim |x|$ and $|B_y| \sim |y|$; the field is zero in the center. The ion propagates along the z -axis.

In the first quadrupole, the net result is that, when the ion crosses a point of the x -axis, it will be focused towards the center and the more far the ion is from the center the stronger is the force acting on it. When it crosses a point of the y -axis it will be defocused. When it crosses any point of the xy -plane it will be focused in the x direction and defocused in the y direction. In the second quadrupole the opposite thing will happen: The y -axis is focusing the x axis is defocussing.

If we set the two (rotated) quadrupoles one after the other in a very short distance, the net result is null. The trick is then to insert a drift section between the two quadrupoles in such a way that the total focalization is stronger than the defocalisation. So, thanks to the drift section and to the fact that the intensity of the

force increases linearly with the distance from the center, the combined effect is focalization. The focusing power is proportional to the length of the drift section and to the strength of the magnetic fields.

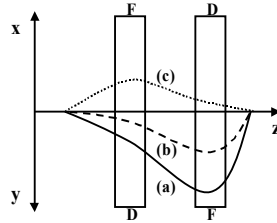


Figure 1.5 – Focusing and defocusing of particles with different starting angles passing through the magnets

In the figure above we have three possible trajectories, starting from the same position, but with different angles. Consider trajectory (b). The particle transverses the first dipole in a position which is double closer to the middle of the dipole than particle of trajectory (a). Since the strength of the field is proportional to the distance, the defocusing power of the first dipole and the focusing power in the second dipole are half than in the case of trajectory (a). The net result is that the two particles land in the same position at the exit.

That is why a pair of quadrupoles focuses: it collects particles that are equal in rigidity but not in angle.

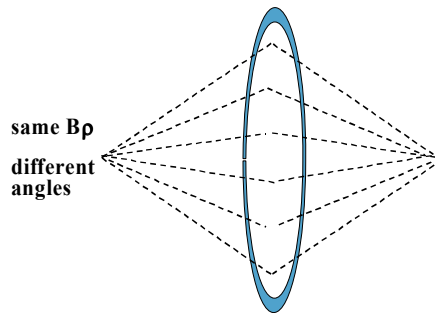


Figure 1.6 – Focussing particles with same $B\rho$ and different angles

1.4.3 Sextupoles

Sextupoles are used to correct for the momentum dependence of the focusing strength of quadrupoles. The field strength of a sextupole is proportional to the square of the distance from the origin.

Chapter 2

Transmission at the Fragment Separator

2.1 The Fragment Separator

The FRS [7] is an achromatic magnetic spectrometer used at GSI for the study of reaction mechanism and radioactive nuclei production. This spectrometer is situated at the exit of the SIS synchrotron and it is composed of four independent stages, each of them consisting of a magnetic dipole and a set of quadrupoles. The quadrupoles determine the ion-optical conditions of the four image planes. The second and fourth image planes are the most important in the achromatic mode because the beam is focused in both transverse directions whereas in the first and third image planes the beam is defocused in one of the transverse directions. The parameters which characterize this achromatic mode are a dispersion of 6.8cm/% in the central image plane and a resolution of $p/\Delta p=1500$.

Two step experiments with FRS allow to produce radioactive beam with very exotic nuclei in the reactions of fragmentation of ^{132}Xe and fission of ^{238}U on the production targets of Be and Pb, respectively. Fully identified residues from these reactions impinge on the reaction target. The fragmentation residues are then isotopically identified in the second section of the spectrometer.

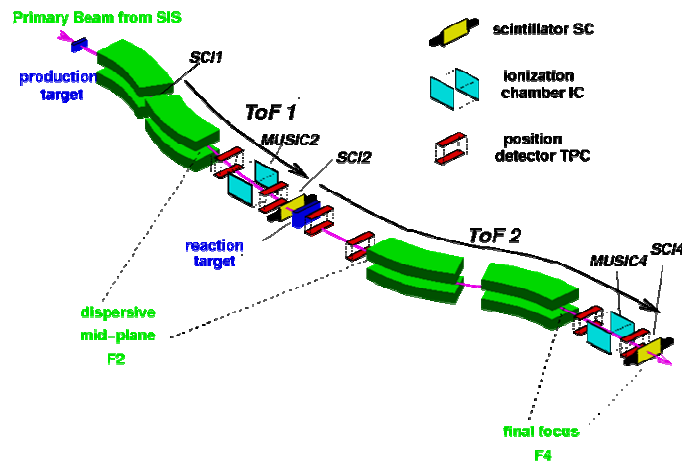


Figure 2.1 – Schematic layout of the FRS showing the dipole magnetic elements and the detector systems used in experiment

The identification of different isotopes produced in the production target can be done by using the relation which correlates the magnetic rigidity of the particles passing through the FRS with its transverse position in the second image plane:

$$(B\rho)_2 = (B\rho)_0 \cdot \left(1 + \frac{x_2}{D_2}\right) \quad (2.1)$$

where $(B\rho)_2$ is the magnetic rigidity of the beam, $(B\rho)_0$ is the magnetic rigidity of the centered beam, x_2 is the transverse position in the second image plane and D_2 is the dispersion for the two first dipole. Two TPC detectors located at the second image planes allow to determine the positions and angles of the particles. The velocity of the particles can be determined from the time-of-flight (ToF) measurements using two scintillator detectors positioned at first and second image planes. An ionization chamber (MUSIC) located at the second focal plane gives the charge identification of the isotopes. All these measurements allow determining the mass of all the isotopes by formula:

$$A = \frac{ZB\rho}{\beta\gamma} \quad (2.2)$$

where A and Z are the mass and the charge of the nucleus, $B\rho$ is the magnetic rigidity and $\beta\gamma$ are the relativistic factors.

The identification of different isotopes produced in the target positioned in the second image plan can be done by using next relation:

$$(B\rho)_4 = (B\rho)_0 \cdot \left(1 + \frac{x_4 - M_4 x_2}{D_4}\right) \quad (2.3)$$

Position and velocity are obtained from TPC detectors positioned at fourth focal plane. Two scintillator detectors positioned at second and fourth focal plane measure ToF in the second part of the FRS. MUSIC chamber gives the charge identification of the isotopes. Using formula 2.2 mass of selected isotope could be obtained.

Characteristic shapes of position distributions at S2 and S4 for different tin isotopes in FRS setting on ^{132}Sn are presented in figure 2.2. The effects of transmission in the first part of the FRS can be seen on the left figure. ^{132}Sn is good centered and its distribution covered the whole focal plane. Distributions of other isotopes are moved to the both sides in the focal plane. Figure on the left shows the position distributions for these isotopes in the last focal plane. They are mainly centered around 3 cm, that the FRS is not well-centered in the second part.

To perform various calculations with these fragments we need to know how many fragments are lost from S2 to S4 focal planes due to ion-optical properties of

the FRS. Monte-Carlo code MOCADI allows us to calculate transmission through the separator and make corrections in our calculations.

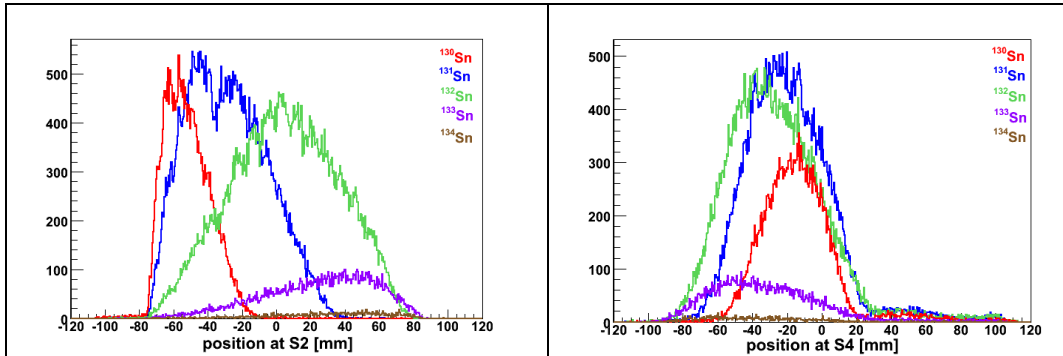


Figure 2.2 – Distribution of different tin isotopes at S2 (left) and S4 (right) focal planes for setting ^{132}Sn

2.2 Beam without dispersion in transversal momentum

An initial beam coming from the SIS and entering the FRS has no dispersion in transversal momentum, so the particles have no angular dispersion. In this case, transmission is 100%. This is easy to understand because the range of $\pm 10\text{cm}$ is within the geometrical acceptance of the FRS and then if one particle can pass the rest of them can pass, also because all have the same features.

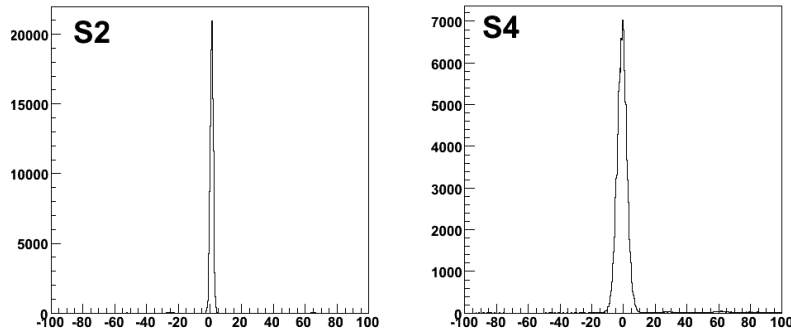


Figure 2.2 – Transversal distribution for primary beam at S2 and S4 planes

2.3 Beam with transversal momentum dispersion: fragmentation reactions

Fragmentation reactions introduce dispersion in the momentum distribution of the particles passing through the FRS. This distribution can be described with a Gaussian function in the 3-momentum coordinate space. The value of the dispersion introduced by the fragmentation reaction was parameterized by Goldhaber by means of the following expression:

$$\sigma^2 = \sigma_0^2 \frac{A_f(A_p - A_f)}{A_p - 1} \quad (2.4)$$

where A_p and A_f are the number of nucleons of the projectile and the fragment, respectively. From this formula we can deduce that the width of the momentum distribution is directly related to the mass difference between the initial projectile and the fragmentation residue.

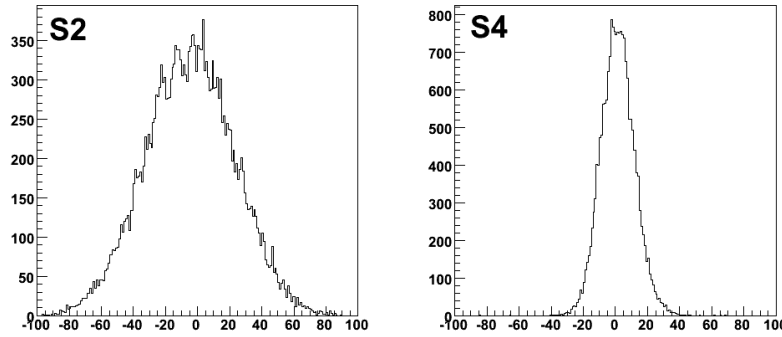


Figure 2.3 – Transversal distribution for fragmentation products at S2 and S4

2.4 Beam with transversal momentum dispersion: Fission reaction

In the case of fission reactions, the transmission of the fission residues depends strongly on the kinematics of the process. Momentum conservation considerations govern the kinematics of this process where the two fission fragments will be produced with equal momentum but opposite direction and isotropically distributed. In the velocity space and in the center of mass frame, the velocity distribution of a fission fragment is represented by the surface of a sphere, the radius of which is defined by the velocity of the fragment. The Lorentz transformation to the laboratory frame gives an ellipsoid as represented in figure 2.4.

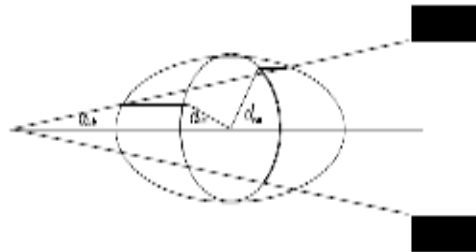


Figure 2.4 – Schematic representation of the fission kinematics

From the analysis of figure 2.4 we can conclude that the angular transmission of the fission residues can be determined if we know the angular aperture of the spectrometer, the beam velocity and the fission recoil velocity.

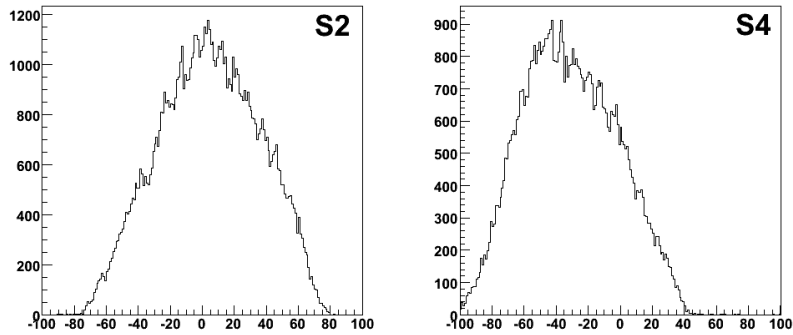


Figure 2.5 - Transversal distribution of fission products at S2 and S4 planes

Chapter 3

MOCADI – Monte Carlo code for the transport of heavy ions through matter within ion-optical systems

The Monte Carlo program MOCADI was the first code capable of tracing an arbitrary phase-space-density distribution of relativistic heavy ions through ion-optical systems taking into account all particle coordinates and higher-order image aberrations as well as atomic and nuclear interaction with matter. It was developed [5] for design studies of the GSI fragment separator FRS. MOCADI is now routinely used for preparation and analysis of experiments with secondary nuclear beams: e.g. for rate estimations, for studying beam properties, separation quality, implantation profiles, optimization of the experimental setup, and transmission studies. It has proven to be an excellent tool for these purposes and all necessary inputs concerning ion-optics and reactions are steadily improved according to experimental results.

3.1 Interaction of heavy ions with matter

When an energetic ion, characterized by its atomic number Z_p , mass number A_p , and ionic charge state q , penetrates through matter, different atomic and nuclear processes can take place. The particle (i) can change its ionic charge state by capturing or losing electrons; (ii) can capture or lose nucleons in nuclear reactions (e.g. charge-changing reactions, fission, fragmentation, electromagnetic dissociation); (iii) will change its kinetic energy and direction as a result of both nuclear and atomic collisions. All these processes change the longitudinal and transverse phase-space density and in case of nuclear interactions also the particle identity.

3.2. Nuclear interactions

Projectile fragments are produced in peripheral nuclear collisions: impact parameters smaller than the sum of the radii of the colliding nuclei lead to abrasion of nucleons, larger impact parameters lead to Coulomb excitation. In both cases the excited nucleus evaporates particles or may fission.

Production cross sections for projectile fragmentation can be well estimated using the semi-empirical parameterizations (EPAX [11]), intranuclear-cascade calculations or abrasion-ablation calculations (ABRABLA [12]). The nuclear absorption can be described by the total reaction cross section. The longitudinal momentum distribution of a specific fragment can be determined from the mean momentum loss in the reaction and from the momentum spread. The Fermi momenta of the abraded nucleons determine the width of the prefragment-momentum distribution. In general the evaporation of nucleons additionally contributes to the momentum distribution of the measured reaction products. The kinematics of the relativistic fission products is determined from the total kinetic energy of the fission process transformed into the laboratory frame. The nuclear interaction is implemented in MOCADI in terms of cross sections and reaction kinematics.

3.3 Atomic interactions

A precise knowledge of the atomic interactions in matter is especially important for efficient in-flight separation of energetic fragments using thick degraders placed at dispersive focal planes ($B\rho$ - ΔE - $B\rho$ separation method). Energy loss, energy-loss straggling, charge-state population, and multiple angular scattering are key parameters to characterize the results of the atomic collisions in matter, and theoretical descriptions of these observables are implemented in Monte Carlo program. Taking into account the practical requirements in high-energy fragmentation experiments we assume that the layers of matter are thick enough to avoid the descriptions of preequilibrium effects.

A first estimation on the ionic charge states of heavy ions can be obtained by the velocity criterion postulated by Bohr: projectile electrons are stripped off in atomic collisions when the projectile velocity exceeds the orbital velocity of the bound electrons. This means that at sufficiently high energies the projectiles are bare or carry only few bound electrons which simplify a stringent comparison with theory.

The mean energy loss and the energy straggling of ions in matter must be known very accurately for selecting the magnetic rigidity of the ion-optical stages following the layers of matter, for the predictions of the transmission properties of the fragments within the optical system, and also for the calculations of the range distributions in special stopping materials.

The energy loss of relativistic heavy ions mainly results from collisions with target electrons. In a first approximation it can be calculated using the relativistic Bethe formula. However, precise energy loss measurements of very heavy projectiles demonstrate large systematic deviations from the results of theoretical calculations based on the first Born approximation. Incorporating the relativistic Mott scattering cross section and the Bloch correction, the stopping power theory yields then a perfect agreement with the experimental data. The energy-loss straggling receives its major contributions from close collisions with target

electrons and from statistical fluctuations of the ionic charge states (charge-exchange straggling). The angular scattering distribution can severely limit the transmission and resolution properties of spectrometers, especially if thick layers of matter are involved. The Coulomb deflection of ions in the field of the target nucleus can be described by a classical treatment for heavy collision systems at all presently available energies.

3.4 Transport through matter within ion-optical systems

In ion optics the transfer function images the initial phase space to any desired position in the system. A widely used approximation for the transfer function is represented by the matrix formalism. The matrix elements are the coefficients of expanded Taylor series. The order of the optical description defines to which order the Taylor series is evaluated. Many ion-optical codes, such as COSY, GICO, MIRKO, Raytrace and TRANSPORT, can be applied to calculate the transfer matrices of any electromagnetic system. The matrices, obtained from these calculations have been implemented in MOCADI to transform the phase-degrader space coordinates of the ions through any selected part of an optical device. By successive application of this transformation one can easily trace a particle through complex ion-optical systems also if the ions interact with matter placed within the device. The theoretical descriptions are applied to modify the coordinates of the particles in case of atomic and nuclear interactions in combination with the established optical imaging. In this way the particles propagate through a system consisting of ion-optical elements and layers of matter.

3.5 Structure and applications of the code MOCADI

The code MOCADI, written in the language C, consists of modules which can be arranged in a desired sequence to realistically simulate a complex experimental setup. The initial coordinates can be randomly selected to represent, for example, the incident projectile beam in front of a target at the entrance of a spectrometer. The atomic and nuclear interactions are simulated in the module 'target'. The particles emerging from the target are then transported through a part of an ion-optical device until the next interaction with matter is introduced. The whole ion-optical device is realistically described by the matrix formalism, the drift lengths, the apertures, the geometrical boundaries of vacuum chambers, and slits. The coordinates of the particles can be recorded and stored at any desired position of the device. These data can be treated like experimental list-mode data. Realistic transmission properties of ions analyzed in complex devices can easily be obtained in this way.

Chapter 4

Simulations and analysis

4.1 MOCADI simulation for calculating transmission of FRS from S2 to S4

In this chapter method for calculating and evaluating transmission in the second part of FRS is presented. Using Monte Carlo MOCADI code simulation of experiment where ^{132}Sn isotope passing through the FRS tuned in three different magnetic settings ^{132}Sn , ^{134}Sn and ^{136}Sn is made. Characteristic position distributions of ^{132}Sn at S2 and S4 for these three cases are presented in figure 4.1.

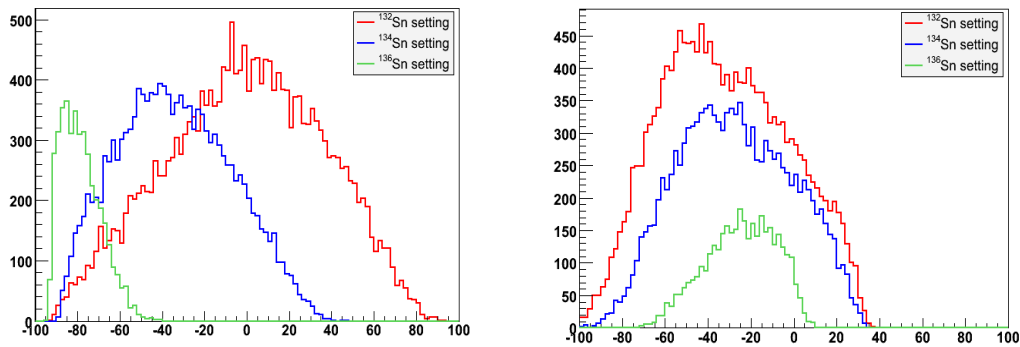


Figure 4.1 – Position distribution of ^{132}Sn isotope at S2 (left) and S4 (right) focal planes in three different settings: ^{132}Sn , ^{134}Sn and ^{136}Sn

Transfer matrices which describe magnetic ion-optical system of FRS were calculated by GICOSY code. Parameters of these matrices together with parameters which describe targets and detectors used in experiment described in section 2.1 are included in input file for MOCADI simulation. Input file were calibrated using calibration files from experiment in order to set a proper values for position and thickness of detectors. Energy losses in the matters in simulation should be the same as in experiment.

Simulation of ^{132}Sn passing through FRS centered on this isotope was made. To discuss obtained results and compare with experimental, three variables are introduced. These are position and angular distributions in x and y angle at S2 and S4 focal plane. All these distributions for experiment and simulation are presented on figures 4.2 and 4.3. It can be seen that they look very similar.

We are very interested in study how to parameterize these distributions in order to see what causes changes in the shapes and positions of them. This allows to make comparison among distributions and see how transmissions are changed.

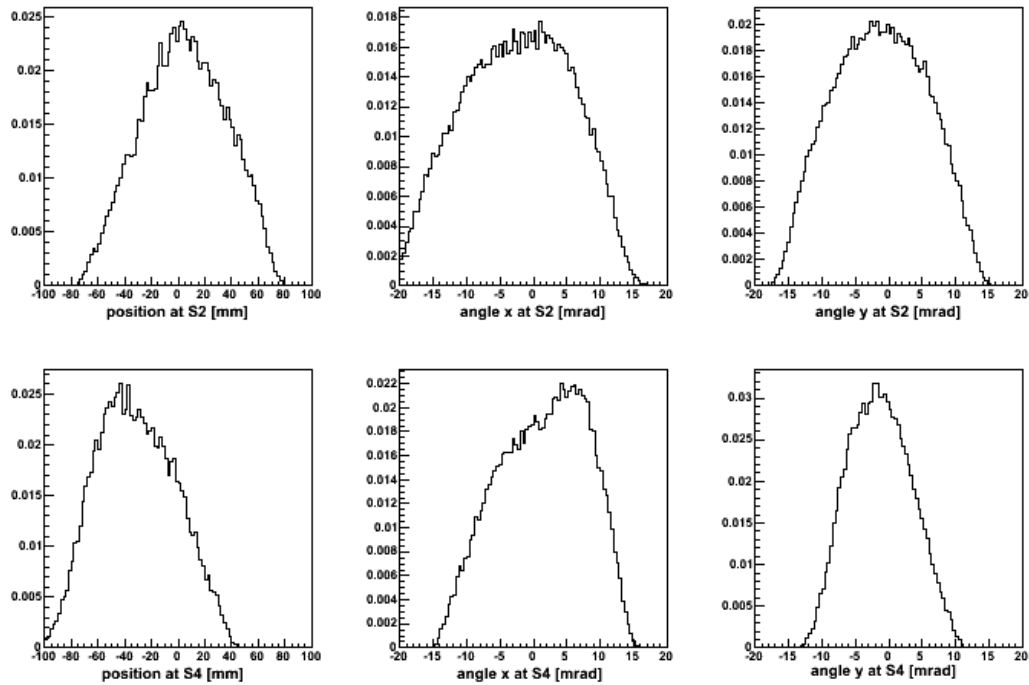


Figure 4.2 – Position and angular distribution in x and y for experimental data

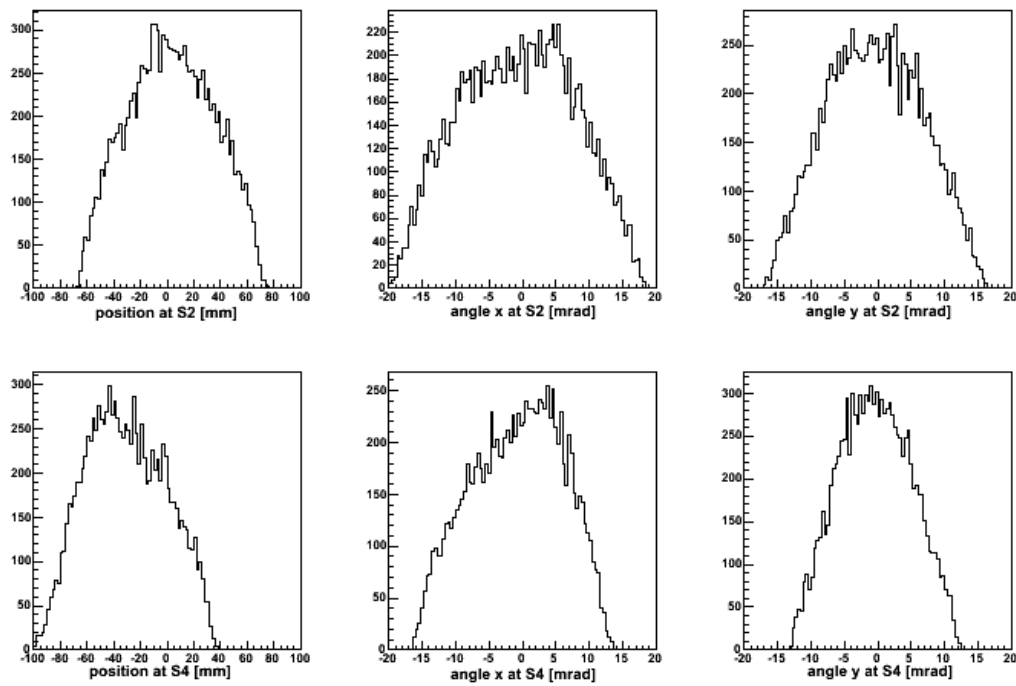


Figure 4.3 - Position and angular distribution in x and y for simulated data

We are looking how to describe these distributions. In order to parameterize them we introduce next parameters: **moments**.

- moment of 1st order presents mean value of distribution
- moment of 2nd order presents RMS or width of distribution
- moment of 3rd order (Skewness) and moment of 4th order (Kurtosis) are coefficients of symmetry of distribution

Main question is how the transmission changes with the changes in these moments. Several sets of different simulations are made where different energies in dipoles (corresponding to magnetic fields in them) are used or restricting the width of distributions closing the slits at S1 and S2 focal plane. Some characteristic results are shown in figure 4.4.

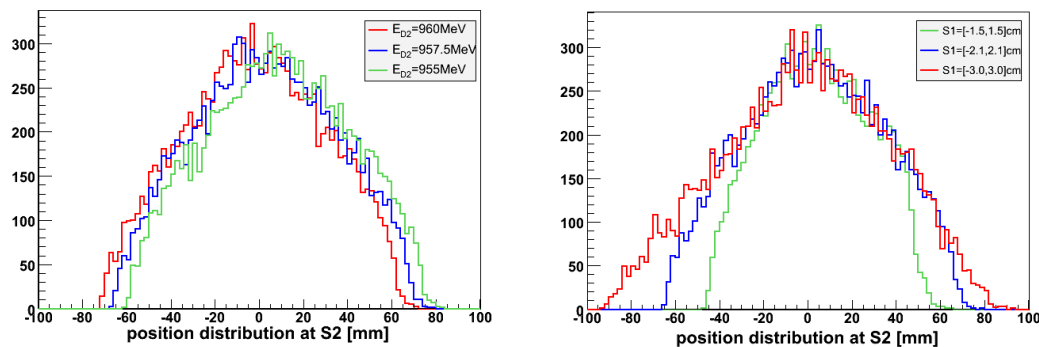


Figure 4.4 – (left) mean value of distribution at S2 in function of energy in the second dipole; (right) width of distribution at S2 in function of closing slits at S1

We introduce deviation of moments as the difference between the values in simulation and experimental ones. This enables us to see how transmission does change with the different values of previously mentioned moments and will allow us to determine uncertainty in the transmission. Systematized results of transmission for several different simulations are presented in next sections and discussed.

4.2 Correlation between position and angular distributions

4.2.1 Position distribution at S2

In order to see if there are any dependencies among distributions we are going to check how changes in one cause changes in the distributions of others. In the first case position distribution at S2 is closing to the center in several intervals.

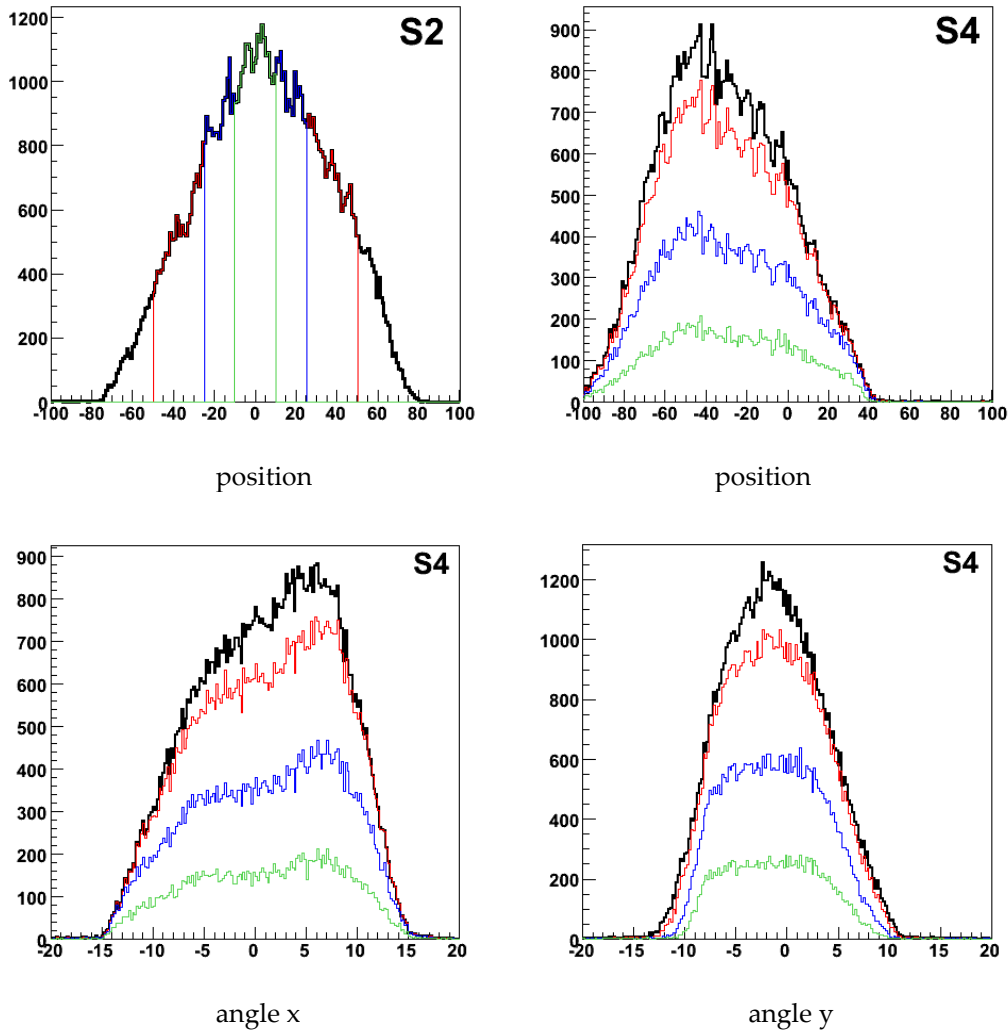


Figure 4.5 – Correlation between distributions for restrictions in position distributions

We see that this closing in distribution cause only reducing the number of events and total statistics.

4.2.2 Angular distribution in x

In this case angular distribution in x at S2 is closing to the center in several different intervals.

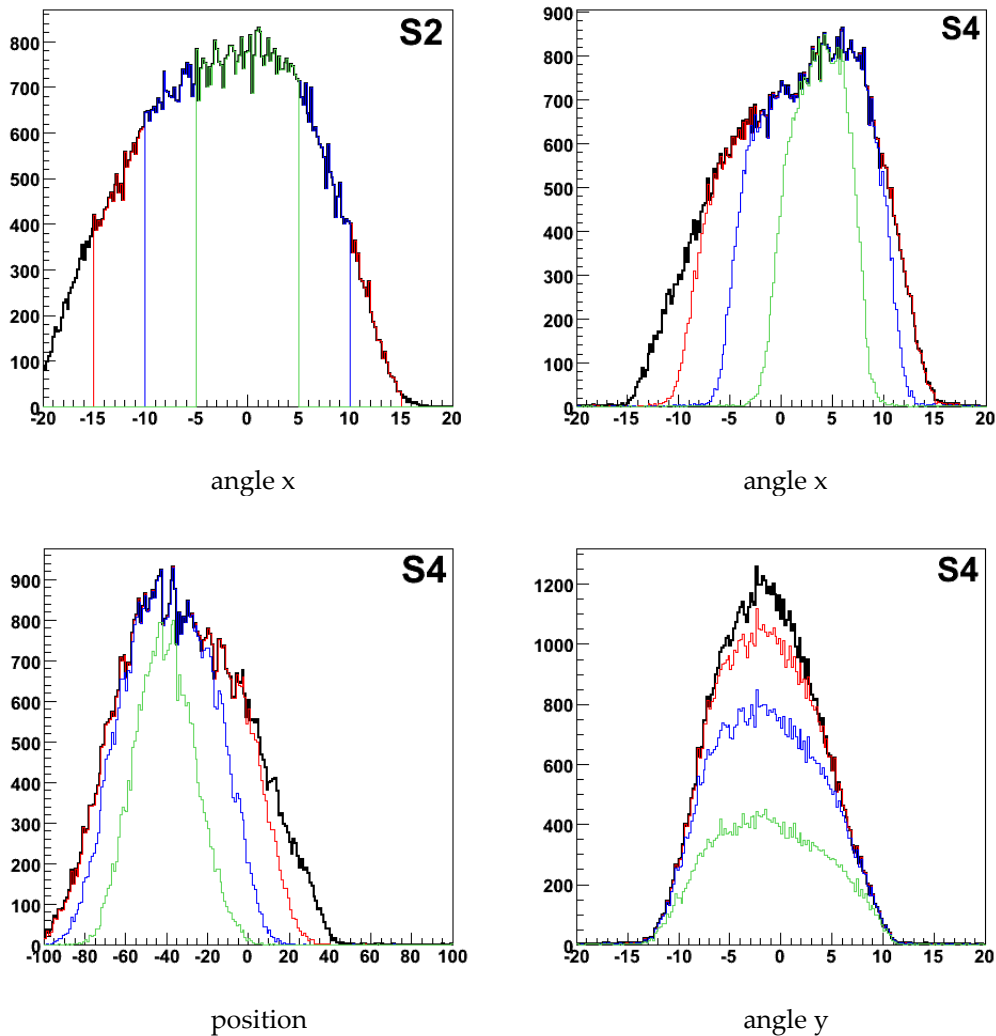


Figure 4.6 – Correlation between distributions for restrictions in angle x distributions

It is evident that changes in angular distribution in x cause changes in width of position and x angular distributions at S4 focal plane, but not on y angular distribution.

4.2.3 Angular distribution in y

Here angular distribution in y at S2 is closing to the center in several different intervals.

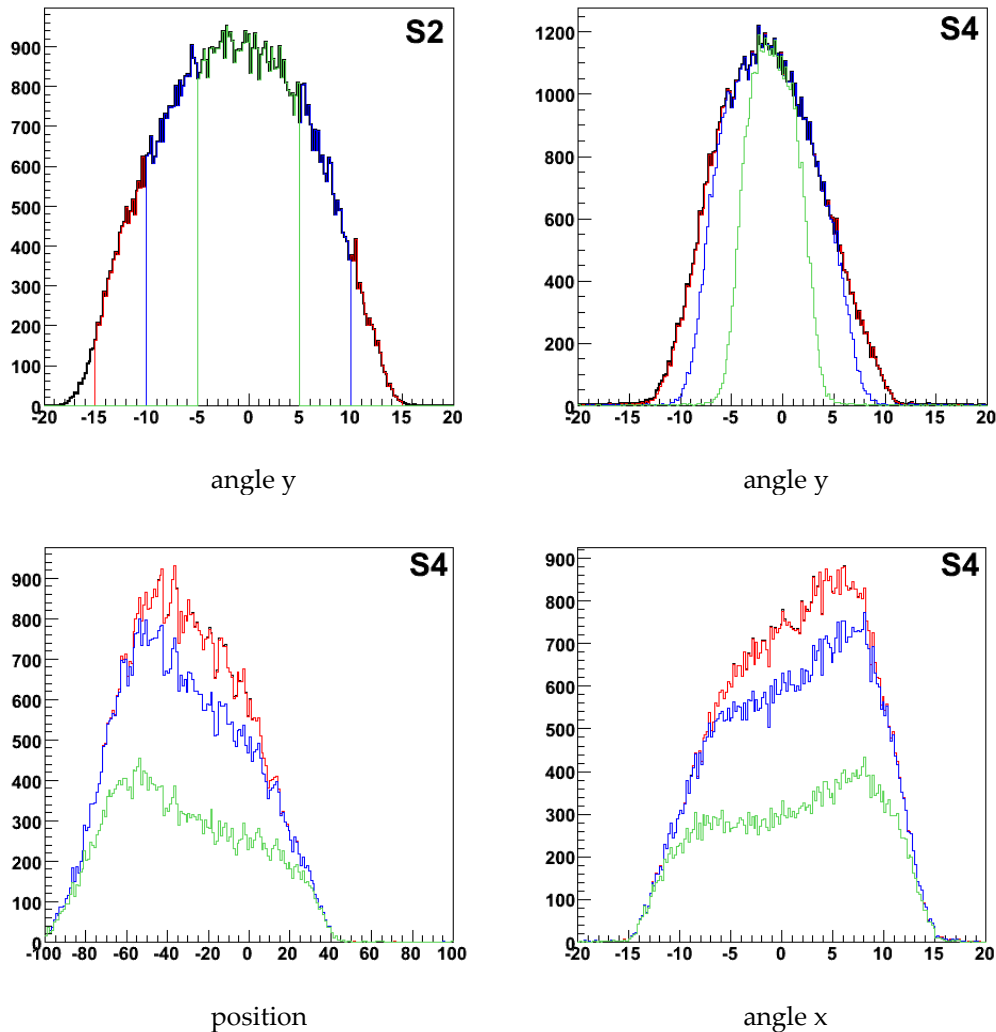


Figure 4.7 – Correlation between distributions for restrictions in angle y distributions

In this case there is correlation only among angular distribution in y at S2 and S4. Closing distribution causes only reducing the number of fragments at final focal plane for other two distributions.

4.2.4 Transmission and restrictions in distribution's widths

In the next plots it is shown how transmission is changed with restriction in distribution's width described in the previous section. The first is shown transmission in function of momentum aperture at S2.

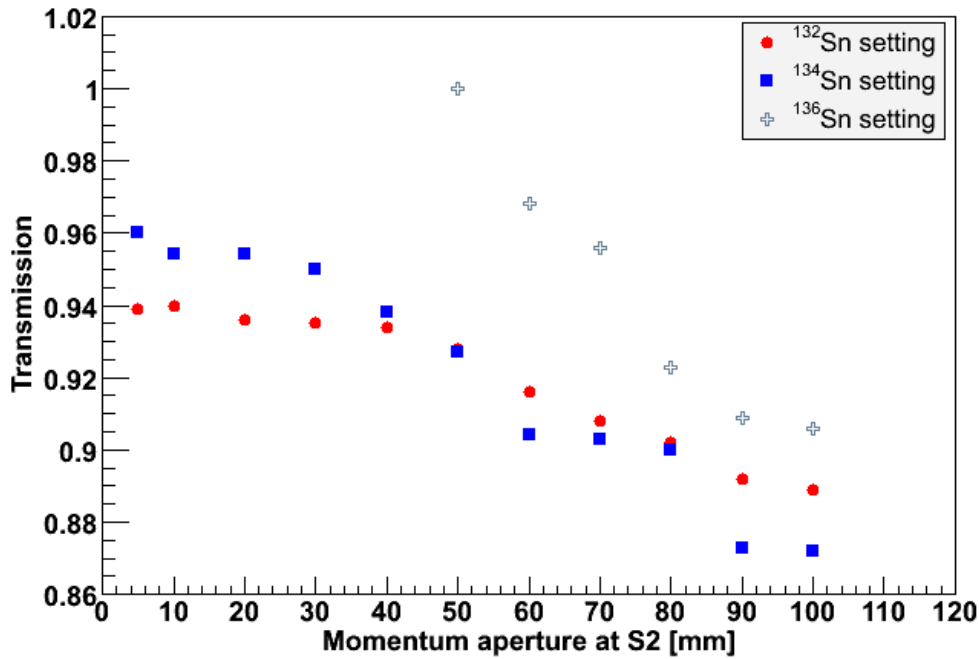
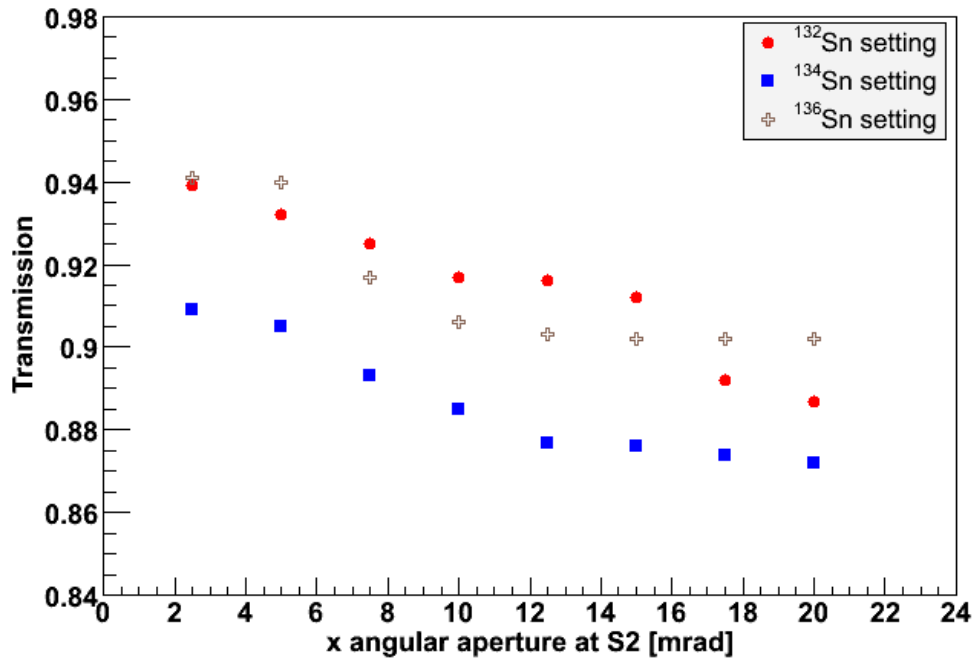
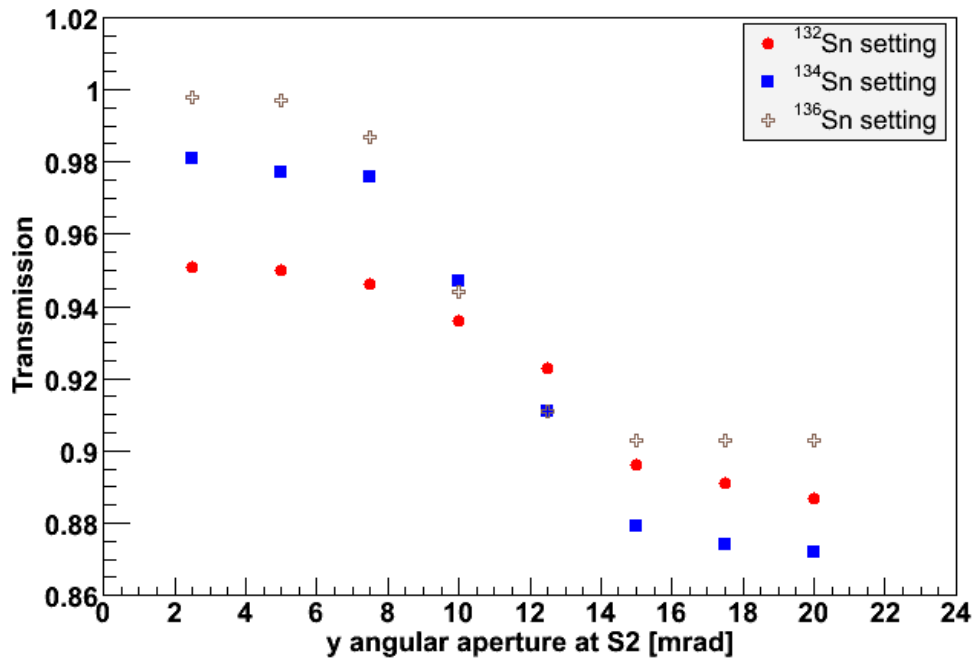


Figure 4.8 – Transmission for restrictions in position distributions

Characteristic slopes on the figure 4.8 show how transmission depends on closing in position distribution at S2 for different settings. Transmission increases with closing aperture to the center of focal plane. Slope is lower as the isotope is near the center of focal plane unlike the others. This means that uncertainty is the smallest for the centered isotope (^{132}Sn setting, see figure 4.8) and increases significantly as it moves far from the centered one (^{136}Sn setting, see figure 4.8).

Figure 4.9 shows how transmission increases with reducing width of angular distribution in x angle. Uncertainties in transmission for fully open and closed aperture are less than 5% for all settings.

Results in the figure 4.10 indicate the existence of a strong dependence of transmission on the reduction in angular aperture for angle y at S2. It is obvious that this distribution should be limited less than 8mrad. This implies that this limitation should be taken into account in the experimental data. Statistics will be reduced, but accuracy will be increased.

Figure 4.9 – Transmission for restrictions in angle x distributionsFigure 4.10 – Transmission for restrictions in angle y distributions

4.3 Evaluation of simulation results

This evaluation should give an answer how our simulation is good. Here will be presented results showing how transmission depends on previously adopted parameters changes. Several sets of different simulation were performed. In one set energies in magnetic dipoles were changed in small steps around experimental values, while in other sets slits at S1 and S2 were closed. Simulated distributions (position and angular) were parameterized using moments introduced in first section of this chapter.

We are studying how much the deviation in moments between measured and simulated distributions affects on transmission. Results are presented and discussed here.

4.3.1 Transmission and deviation from the mean position of distribution at S2

In this set of simulation, energy in the second dipole was changed around experimental value (957.61MeV) in small steps (± 2 MeV). This affects only on position distribution at S2 focal plane which 1st order moment or average position moves (see figure 4.4, left). There is no affects on the other distributions and their moments.

Figure 4.11 shows how transmission is changed with different average position of distribution at S2. To evaluate transmission in this case it is much better to see how it is changed with the deviation in average position between measured and simulated distributions ($x_{sim}-x_{exp}$).

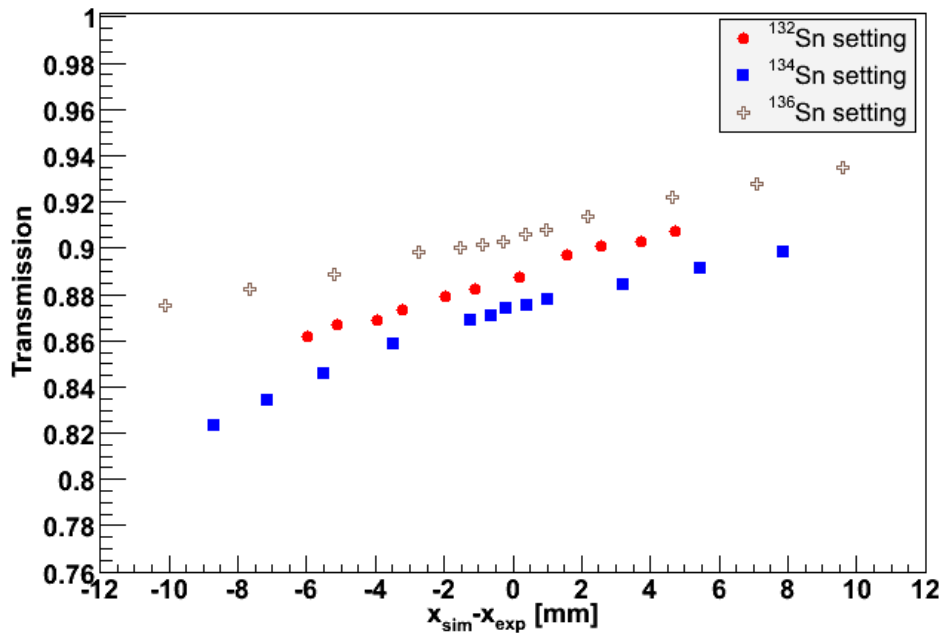


Figure 4.11 – Transmission vs. deviation in average position at S2

Transmission dependence on the deviation in average can be characterized by the slope which can be fitted with linear fit. Figure 4.12 shows the results of this fit which allows us to quantify how transmission changes with deviation in mean position. This means that we can determine the uncertainty of transmission if we know for how much simulated mean position deviates from measured.

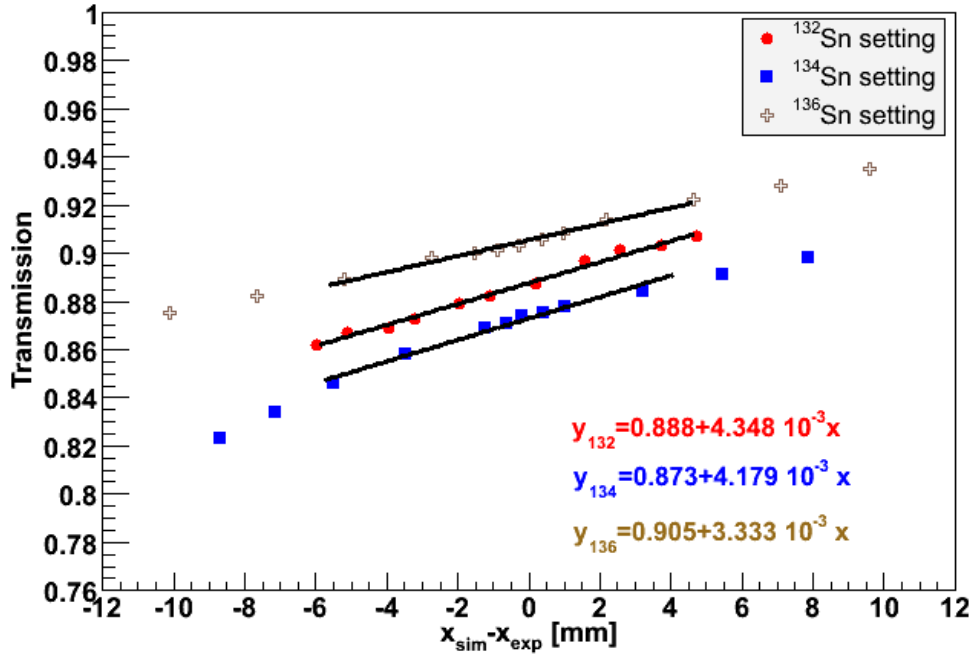


Figure 4.12 – Results of linear fit of transmission's dependence on deviations in average position between measured and simulated distributions

Slope is greater for centered isotope, less for the others. For example, if average position of simulated distributions deviates from the average position of measured distribution in some taken interval $[-3\text{mm}, 3\text{mm}]$ error is 3% for ^{132}Sn isotope in the ^{132}Sn setting, 2.5% in the setting ^{134}Sn and only 2% in the setting ^{136}Sn .

4.3.2 Transmission and width of distribution at S2

In the second set of simulations slits at S1 focal plane were closed from $[-3\text{mm}, 3\text{mm}]$ to $[-1\text{mm}, 1\text{mm}]$ in order to see how this affects on distributions at S2 and S4, and transmission of the second part of the FRS. This change affects only on width (RMS) of position distribution at S2 focal plane (see figure 4.4, right). There is no significant affects on the other distributions and their moments. Figure 4.13 shows how transmission changes with the deviation in width between measured (RMS_{exp}) and simulated (RMS_{sim}) distributions.

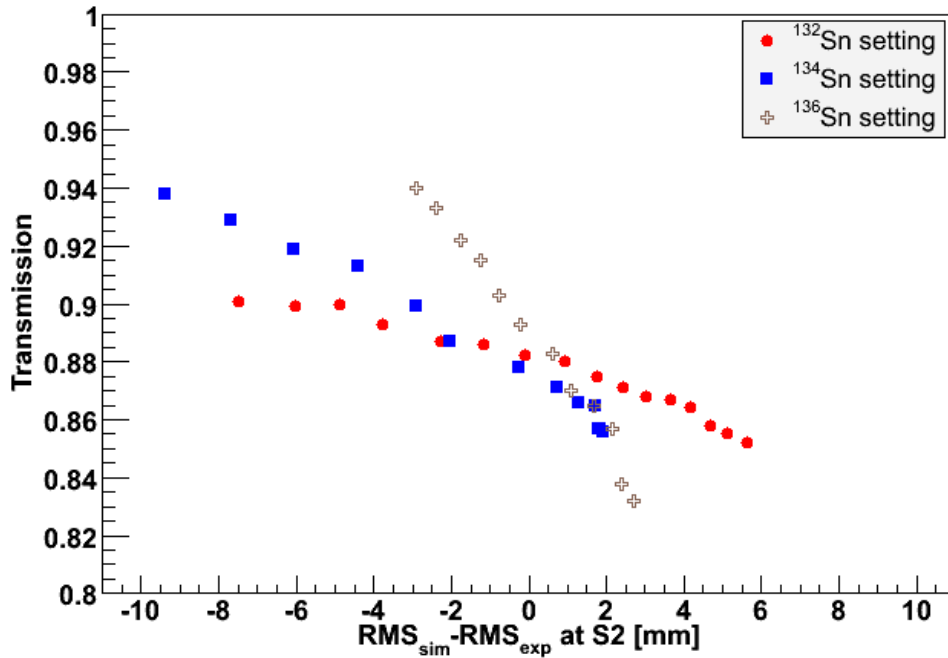


Figure 4.13 – Transmission vs. deviation in width of distributions at S2

Characteristic slopes presented in figure 4.13 indicate that transmission depends on the deviation in width of distributions less for the centered isotopes than the others. These slopes allow us to estimate the error of transmission if width of simulated distribution deviates from measured for some value. For the allowed interval of deviation $[-3\text{mm}, 3\text{mm}]$ error is 1% for ^{132}Sn isotope in the ^{132}Sn setting, 4% in the setting ^{134}Sn and 10% in the setting ^{136}Sn . In other words, width of simulated distributions and its deviation from measured is very important for non-centered isotopes, where small deviations cause great uncertainty.

4.3.3 Transmission and average position of distribution at S4

In this set of simulations, energy in the last two dipoles was changed in small steps around experimental one. This affects only on the average position of the simulated position distributions at S4. Affect on the 2nd order moment is not possible to systematize. Results presented in figure 4.14 show how transmission is changed when average position of simulated position distribution at S4 (x_{sim}) deviates from average position (x_{exp}) in measured distribution. We can see two characteristic behaviors of transmission in function of deviation of average position. The first is that the transmission is mostly constant if mean position of simulated distribution is greater than measured one. Second is appearance of a great drop as soon as the average position in become less then in experiment.

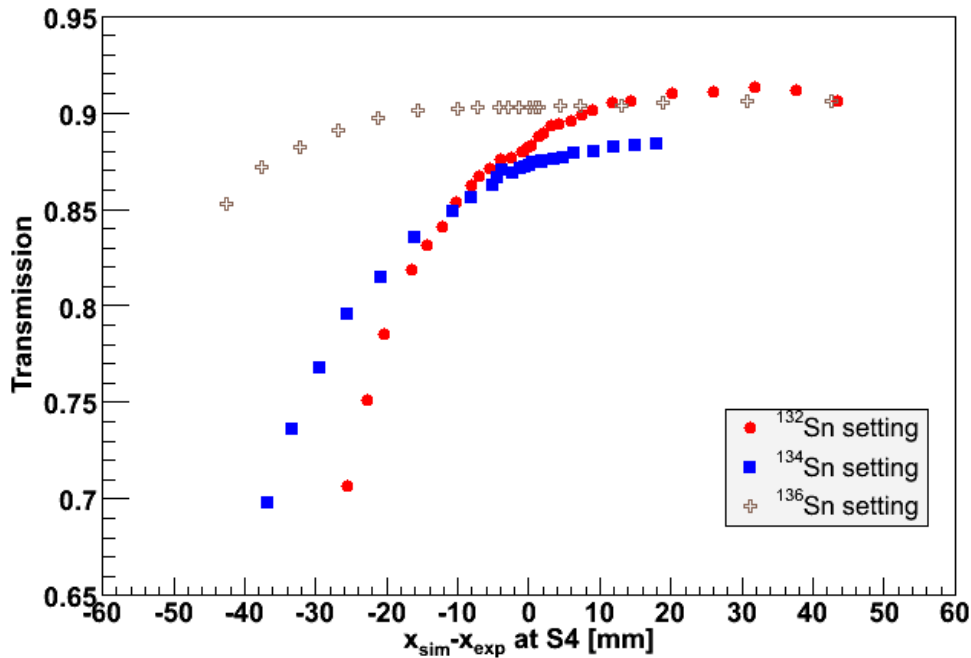


Figure 4.14 – Transmission of the second part of FRS in function of deviation in average position between measured and simulated position distribution at S4

Drop is greater for the centered isotope and decreases as the mean position of distribution is far away from the center. This means that for the particular deviation in average position, transmission is changed faster for isotope in the setting centered on it than in the others. In order to systematize this drop we adopt the criteria of 1%, 3% and 5% of the value of transmission obtained in case where mean position is the equal with the experimental one. Figure 4.13 shows how much deviation in average position is allowed for one isotope in three different settings. In the setting ^{132}Sn error in transmission reaches 1% if mean position in simulation deviates from measured by 4mm. For other two settings ^{134}Sn and ^{136}Sn , this error is reached for deviation 6mm and 20mm, respectively. If we increase selected uncertainty on 3% or 5% for example, these deviations also increase as it is shown in figure 4.15.

These criteria allow us to reliable select possible deviation of average position between simulated and measured distributions so that the transmission is within pre-defined uncertainties.

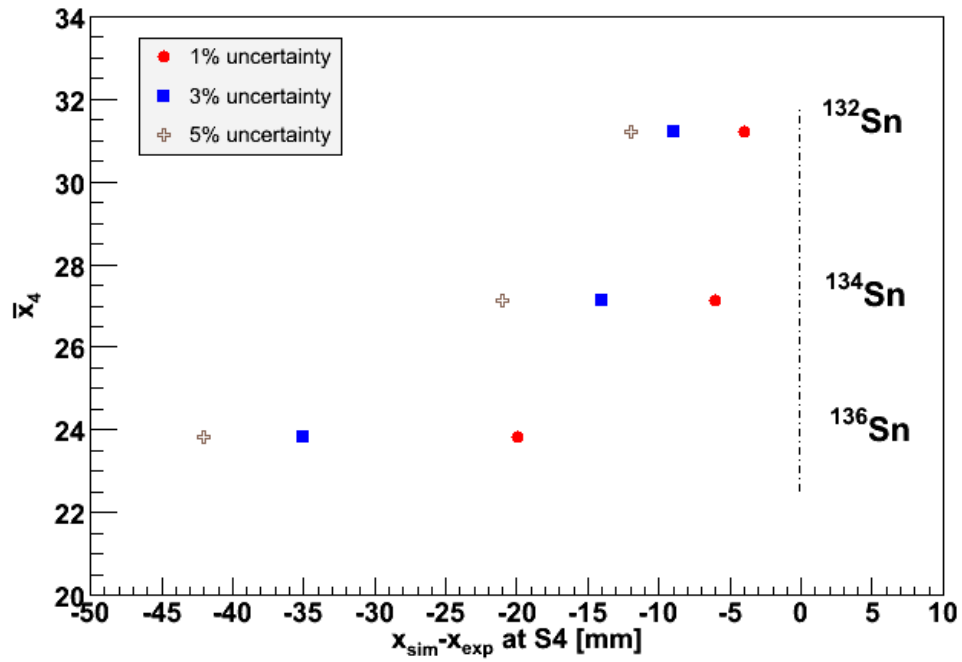


Figure 4.15 – Allowed deviation in average position between simulated and measured distributions for selected uncertainties of transmission

Chapter 5

Summary and conclusions

In this work we have described a general purpose of MOCADI simulation which can be used for calculating the transmission through magnetic spectrometer such as Fragment Separator at GSI. We have applied different sets of simulations to evaluate transmission in the second part of the FRS. The idea was to parameterize angular and momentum distributions in order to be able to compare simulated with measured distributions. We used moments (average position, RMS, Skewness and Kurtosis) to quantify distributions and get the answers how transmission is changed if some parameter which describes simulated distributions deviates from the experimental one.

In simulations we have changed energies in dipoles and closing apertures at focal planes to see how moments are changed and what final affect on the transmission is.

1. Correlation between position and angular distributions

In the first set of simulations we reduce the position and angular aperture of distributions to study what is affect on each other. Only reducing the width of angular distribution in angle x at S2 affects on width of position distribution at S4. Closing the aperture in the other distributions only reduce the statistics.

2. How does this reduction in width of distribution affect on transmission?

There is a strong dependence of transmission on the reduction in the width of angular distribution in angle y at S2. It is necessary to limit this distribution less than 8 mrad in order to increase accuracy of transmission.

Transmission shows characteristic slope in function of reducing the aperture of distributions. These slopes tell us how transmission is sensitive on apertures at S2. For centered isotope this slope is small, with tendency to increase as isotope is move away from centered one. This allows us to calculate uncertainties of transmission.

3. How does deviation in mean position at S2 between simulated and measured distributions affect on transmission?

In this set of simulation we change the energy in the second dipole. This affects only on average position of distributions which deviates from measured average position. There is linear dependence on this deviation, which can be fit by polynomial function 1st order. The slope tells us how fast transmission is changed with the deviation from average position.

4. How does deviation from in width of position at S2 affect on transmission?

Closing the slits at S1 focal plane affects on the width of distributions, closing cause reducing the distributions. There is linear dependence on this deviation, which can be fit by polynomial function of the 1st order. The slope tells us how fast transmission is changed with the deviation. Slope is lower for centered isotope and increase as distribution is moving away from the center of focal plane.

5. How does deviation from mean position at S4 affect on transmission?

In the last set of simulations we changed the energy in the last two dipoles which cause the deviation in average position at S4 focal plane. Transmission is mostly constant when average position of simulated position distribution is greater than in the experiment. However, if simulated average position is less than measured, transmission is characterized by great drop, which is greater for the centered isotope. In order to systematize the affect of this drop on the transmission we introduce strict criteria how much average position of simulated distributions can deviate from measured one as transmission is not changed more than selected uncertainty.

We conclude that presented moments qualitatively describe momentum and angular distributions and allow us to calculate transmission with certain accuracy. Deviations in certain moments between measured and simulated distributions are systematized. This allows us to calculate transmission with certain error with capability that moments which describe simulated distributions are able to deviate in some certain interval from moments which describes experimental distributions.

Appendix

Here are presented momentum and angular distributions for ^{132}Sn isotope passing through the FRS in three different magnetic settings ^{132}Sn , ^{134}Sn and ^{136}Sn .

a) ^{132}Sn isotope in FRS setting ^{132}Sn

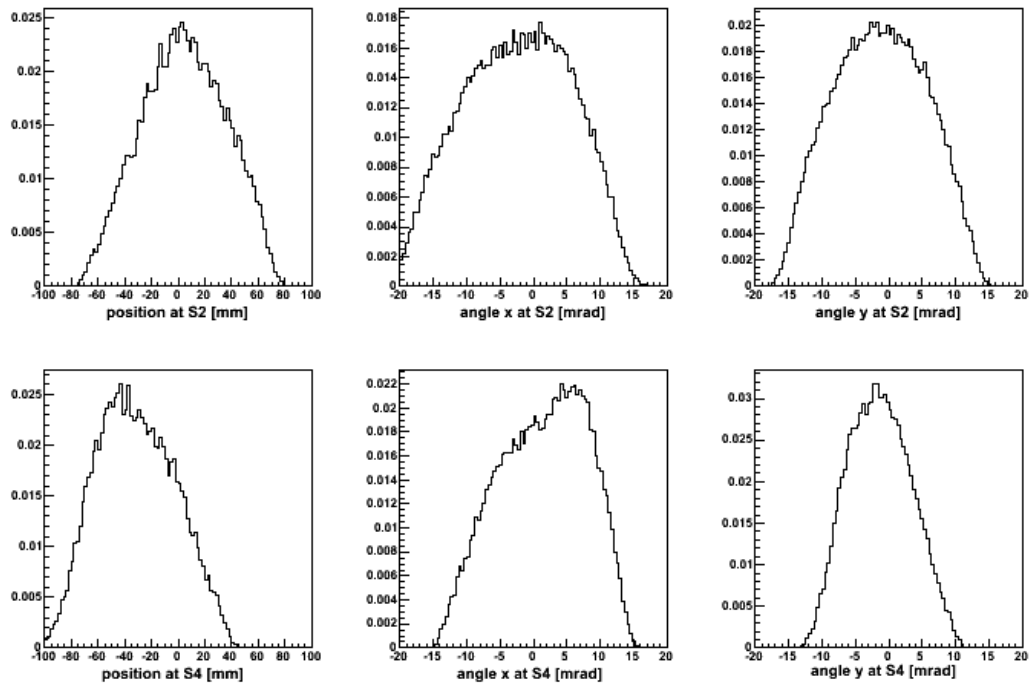


Figure A.1 – Position and angular distribution in x and y for experimental data

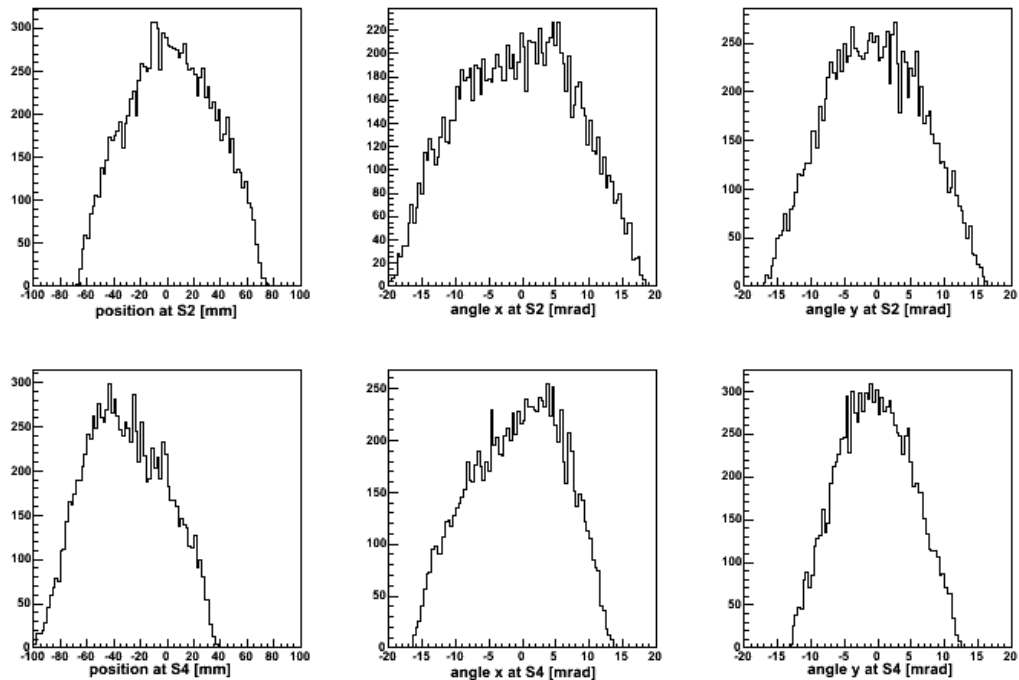


Figure A.2 – Position and angular distribution in x and y for simulated data

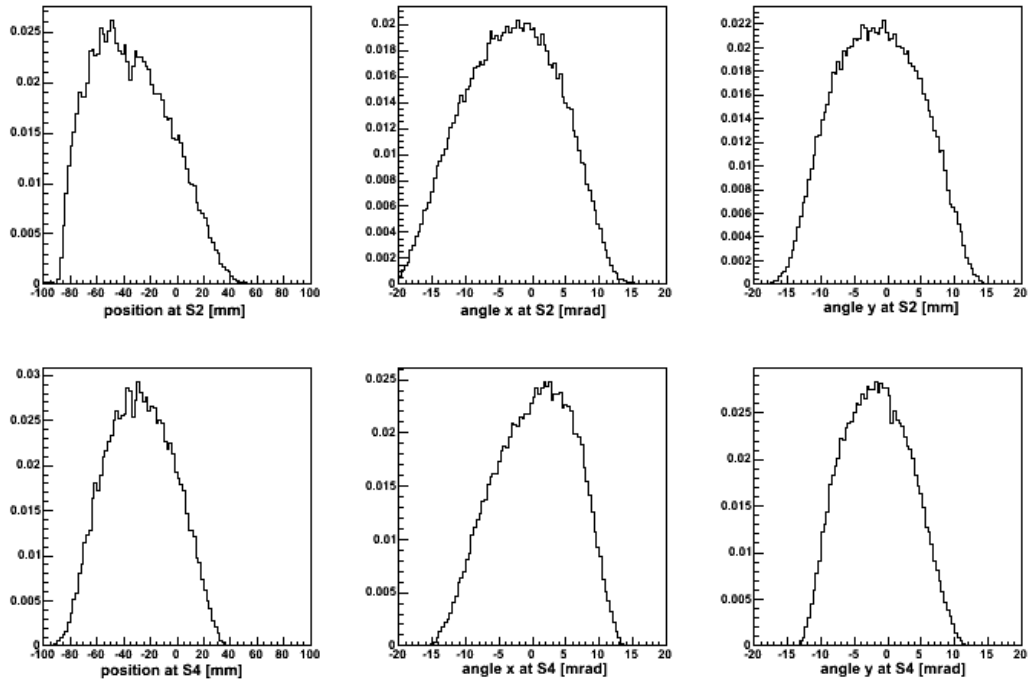
b) ^{132}Sn isotope in FRS setting ^{134}Sn 

Figure A.3 – Position and angular distribution in x and y for experimental data

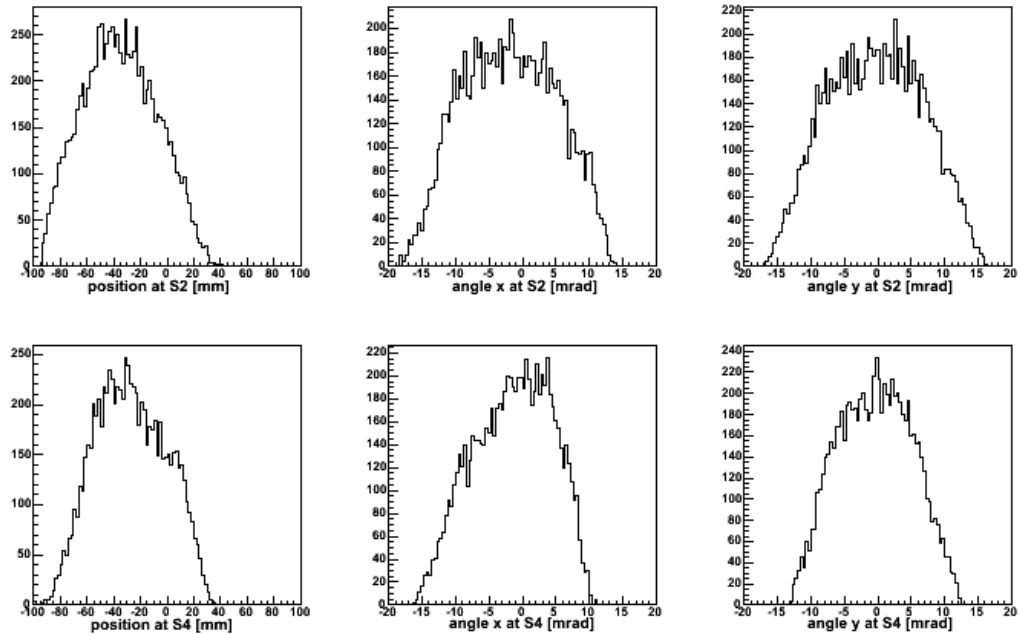


Figure A.4 – Position and angular distribution in x and y for simulated data

c) ^{132}Sn isotope in FRS setting ^{136}Sn

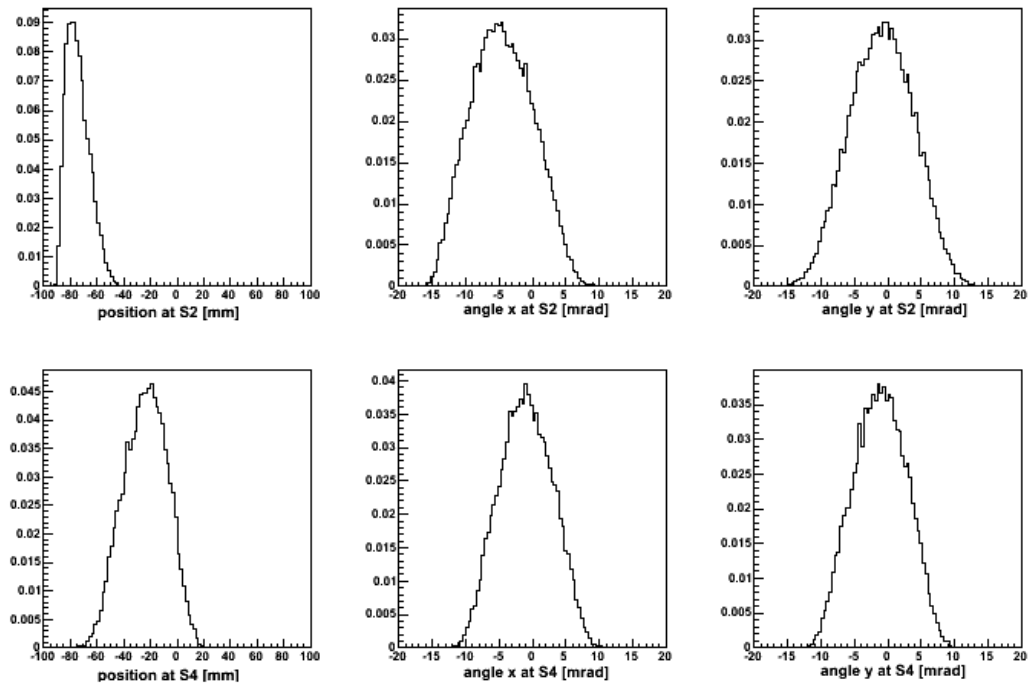


Figure A.5 – Position and angular distribution in x and y for experimental data

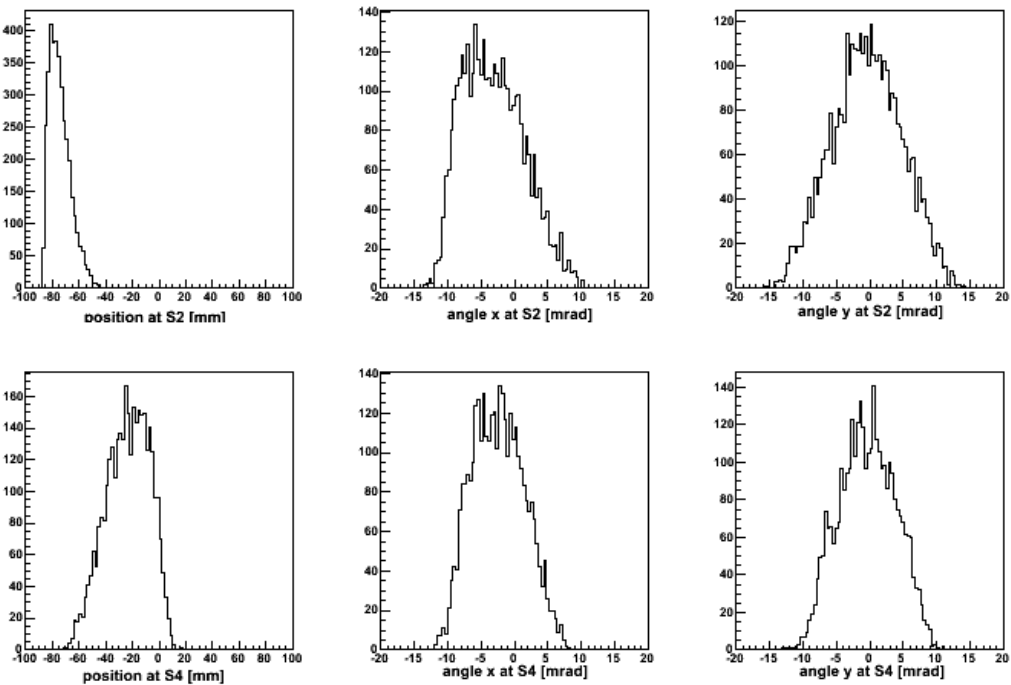


Figure A.6 – Position and angular distribution in x and y for simulated data

Bibliography

- [1] GSI home page, www.gsi.de
- [2] RIKEN home page, www.riken.go.jp/engn
- [3] GANIL home page, www.ganil-spiral2.eu
- [4] K.L. Brown, *Adv. Particle Physics* 1 (1967) 71.
- [5] N. Iwasa et al, *Nucl. Instr. Meth. Phys. Res. B* 126 (1997) 284.
- [6] H. Wollnik, *Manual for GICO* (University of Gießen, 1990).
- [7] H. Geissel et al, *Nucl. Instr. Meth. Phys. Res. B* 70 (1992) 286
G. Munzenberg et al, *Nucl. Instr. Meth. Phys. Res. B* 70 (1992) 265
- [8] David C. Carey, *The Optics of Charge Particle Beams*, Harwood Academic Publishers, 1987).
- [9] Maria Valentina Ricciardi, *Ion optics*, Lessons of Karl-Heinz Schmidt
- [10] ALADIN web page, www-aladin.gsi.de/www/kp3/aladinhome.html
- [11] K. Summerer and B. Blank, *Phys. Rev. C* 61 (2000) 034607
- [12] J.-J. Gaimard and K.-H. Schmidt, *Nucl. Phys. A* 531 (1991) 709